POLITECNICO DI TORINO

**Master Degree course
in Sustainable Nuclear Energy**

Computational Thermal Fluid Dynamics

Friction factor analysis of a staggered tube bank in cross flow

Professor
Roberto BONIFETTO
Antonio FROIO
Andrea ZAPPATORE

Student
Luigi BUTTICÈ
Federico PATI

Academic year 2023/2024

Contents

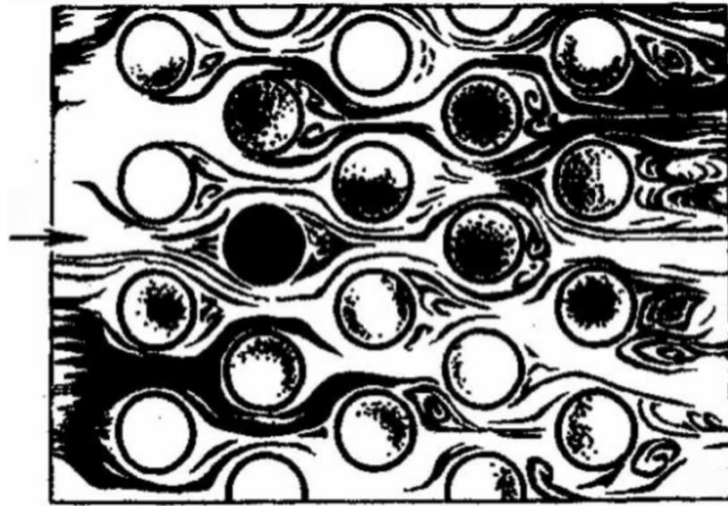# Chapter 1

Introduction

Figure 1.1: Staggered Tube Bank [2]

This study aims to analyze turbulent flow properties, focusing particularly on the calculation of the friction factor exhibited by water when flowing across a staggered tube bank. Computational Fluid Dynamics (CFD) simulations were systematically executed to investigate the friction factor, pressure distribution, and velocity field over the tube bank sample in different Reynolds number. Additionally, properties of the computational model, such as y+, will be scrutinized to ensure the accuracy of the model and to avoid conditions that would invalidate the results.

In a CFD analysis, it is really important, before starting with simulations, to conduct a physical analysis on the main properties of the flow during the passage through the bank of tubes. The elementary cell can be schematized as a converging-diverging nozzle characterized by a throat section (between the two tubes). From a physical point of

view, following an expansion in the converging duct (between the two tubes), there is, subsequently, a compression of the fluid, which implies that:

1) The maximum velocity is located at the throat.

2) Regarding pressure: the maximum is located at the points of stagnation ahead of the tubes, point in which the flow stops isentropically at stagnation conditions where pressure is maximum.

To ensure alignment with existing experimental trends documented in literature, water was employed as the fluids of interest. Above all, since our main reference is the experimental work done by Zukauskas on 49 different staggered tube banks, with different working fluid but with constant density. So it is very simple to fulfill this condition with water but not with air. Subsequently, the Friction Factor, a key parameter, was studied as a function of Reynolds Number (Re), with comparative analyses conducted by Zukauskas work.

To ensure a good prevision of the property of the turbulent flow, as in this case, the examination of the continuity, momentum, and energy equations was conducted using the 'Realizable two layer k-ϵ model'.

A non-uniform grid was generated, incorporating local refinement near the walls to capture the significant modifications induced by the tube geometry. As regard the wall, it is very important to ensure that Y+ parameter does not overcome 5, otherwise you would enter in the buffer layer region.

It will be examinate also the grid convergence of the results through the 'Richardson Extrapolation' showing a pretty good converge of the results both changing base size and number of prism layer.
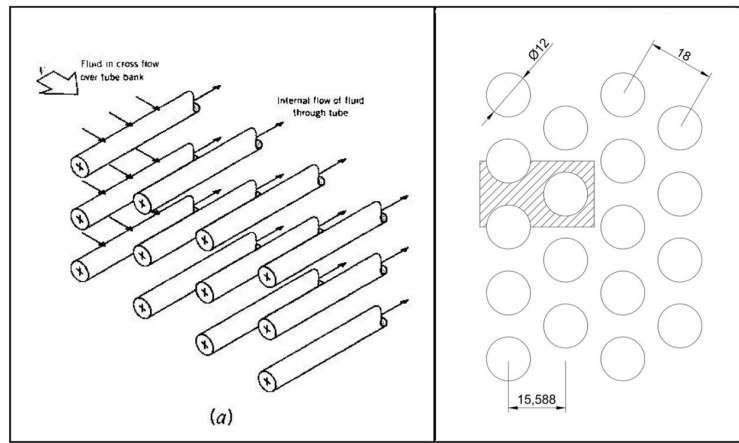
Chapter 2

Geometry and material

Figure 2.1: (a) 3D Prospective and (b) front view of the staggered bank. All dimensions are in millimetres [2]

As said before Zukauskas' values are obtained considering a constant density fluid, so, for this case, we cannot use air as work fluid, because at high Reynolds air overcome the Mach transition number to compressible state, as a consequence we would not have the possibility to compare the results.

Geometrical Pipes Data:

- Pipes Diameter D = 6 mm

- Horizontal distance between the centers of two pipes $S_L = 15.588$ mm

- Vertical distance between the centers of two pipes $S_T = \frac{\sqrt{3}}{2} S_L = 18$ mm

- Diagonal distance $S_D = S_T = 18$ mm

- Longitudinal Pitch $P_L = S_L/\mathrm{D} = 1.3$ [-]

- Transverse Pitch $P_T = S_T/\mathrm{D} = 1.5$ [-]

Thermophisycal fluids properties: Water :

- Dynamic Viscosity = 8.9E-04 Pa*s

- Density = 997 kg/m³

From figure 2.1, moreover it is possible to notice the fundamental cell that will be use as computational domain for our simulation.

Chapter 3

Simulation setup

3.1 Computational Domain

Given the focus of our study on the fully developed condition, the computational domain represents only a cell of entire tube bank, hence, we operated within a 2D domain. This design is intentional, aiming to focus on its periodicity. Consequently, our simulation effectively represents an indefinitely staggered tube bank.
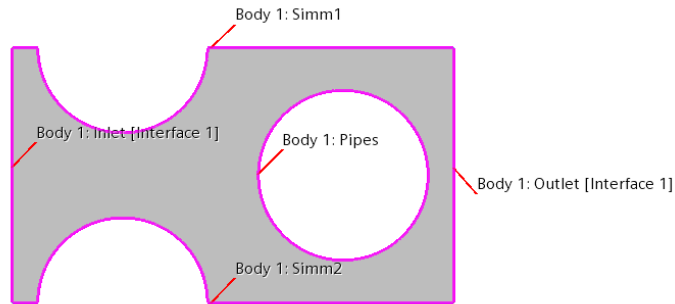
3.2 Boundary Condition

Figure 3.1: Boundary Condition

The distance among each pipe can significantly affect the solutions. As a consequence, almost all correlations in the literature use P_T and P_L to discern the different effects of the geometry on the main flow. To analyze the effects of our particular geometry, and particularly to meet the demand for fully developed turbulent flow, we chose to implement an interface (fully-developed interface) between Inlet and Outlet. Conversely, we applied the 'wall' boundary condition (no-slip condition) on the pipe surfaces and symmetry on the top and bottom planes.

The property of the interface that were possible to change were 'pressure jump' or 'mass flow rate'. Of course we chose 'mass flow rate' option through which we derive the various numbers of Reynolds to vary from which will plotted the friction factor. For outlet boundary condition we implemented a "Pressure Outlet"

3.3 Turbulence Model

The realizable two layer k-ε turbulence model offers several advantages over standard models in computational fluid dynamics (CFD). It demonstrates improved accuracy in predicting the spreading rate of planar and round jets,rotation of the main flow in the presence of curved walls, as well as enhanced performance in flows involving rotation, streamline curvature, adverse pressure gradients, separation, and re-circulation. Additionally, realizable k-ε models exhibit significant enhancements over the standard model in scenarios featuring strong streamline curvature, vortices, and rotation (as our problem).

Studies have shown that the realizable model outperforms other versions of the k-ε model in various validations of separated flows and those with complex secondary flow features. However, it has limitations, particularly in situations where the computational domain contains both rotating and stationary fluid zones. This can lead to the production of non-physical turbulent viscosity due to the inclusion of mean rotation effects in the definition of turbulent viscosity. [1]

Hence, the choice of the realizable k-ε model is theoretically motivated by its superior performance in predicting reliable results for scenarios pretty similar to our case. Detailed explanations of the model can be found in publications by Tsan-Hsing Shih and Jiang Zhu, who first introduced this model [3].

An important consideration during the using of a turbulent model that involve prediction of properties that depend on the wall, is the Y+ parameter. In all simulation we have changed the parameter 'near wall thickness' in order to ensure a value of Y+ smaller than 1. However we have noticed that the simulation results did not change if Y+ was higher than 1 but smaller than 5, in fact k-ε is not a 'low Y+', so the important thing is avoid the buffer layer and so the maintenance of the Y+ below 5. For this reason for our simulation we have used an high number of prism layer like 10.
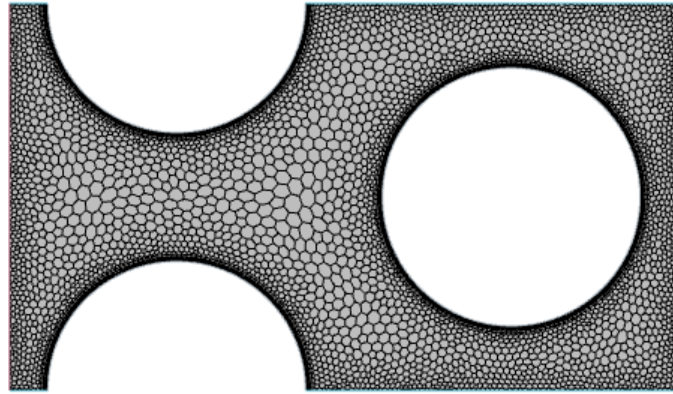
Chapter 4

Mesh generation

Figure 4.1: Definitive Mesh

In order to solve the problem, is required a discretization of the domain. Considering the 2D hypotheses, we can employ the *Automated Mesh 2D* operation, selecting polygonal mesh and also prism layer mesher. This last option adds prismatic cell layers adjacent to wall boundaries, which are essential for accurately resolving the boundary layer and the velocity gradient of the flow near our pipes.

When selecting the most appropriate mesh, it is important to consider both result accuracy and computational cost. A excessively fine mesh may consume significant computational time for a marginal improvement in results, while an overly coarse mesh can yield inaccurate outcomes. Achieving a suitable balance between these considerations can be accomplished through a grid independence study.

Starting from a common base, different meshes were generated varying the base size or the prism layer parameters. These are the most influential parameters,leading us to focus on them our grid independence study.

For both the analyses proceed in a analogous way:

- **Base size:**

  Starting from the finest base size of 0.3 mm, we choose other three different meshes, simply doubling that dimension and consequently the number of cells halve each time. For a fixed number of prism layers, the chosen base size are: 0.3 mm, 0.6 mm, 1.2 mm, 2.4 mm.

  Then, the grid refinement ratio is $r = 2$.

  Setting the Reynolds number at $Re = 2e5$, we can compute the pressure drop ΔP for each discretization. From this value we can compute the *order of convergence* as follows:

  $$p = ln(\frac{\Delta P(1.2mm) - \Delta P(0.6mm)}{\Delta P(0.6mm) - \Delta P(0.3mm)})/ln(r)$$

  Finally, using the *Richardson Extrapolation*, we can obtain an higher-order estimate of the continuum value at zero grid spacing, computed with the formula:

  $$\Delta P_{h=0} = \Delta P(0.3mm) + \frac{\Delta P(0.3mm) - \Delta P(0.6mm)}{r^p - 1}$$

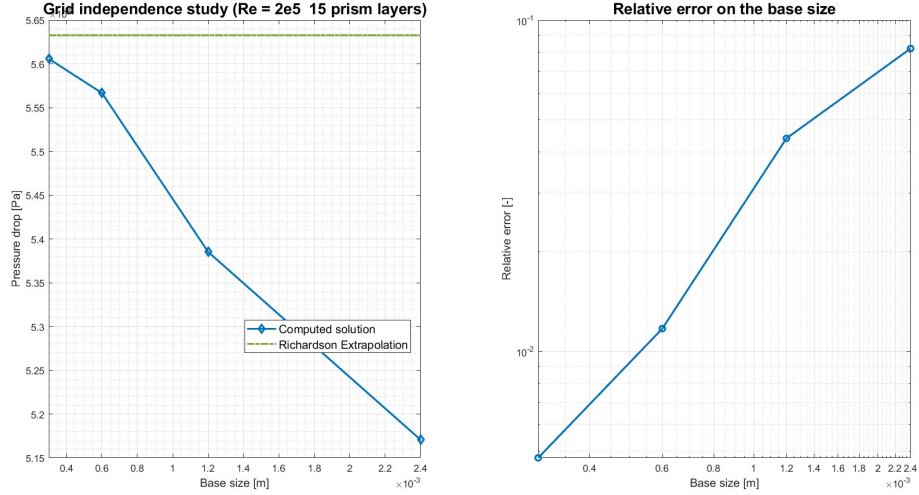 The solution give us a most accurate value to compare our result with.

Figure 4.2: (a) Grid independence on the base size; (b) Relative error

  The two plots in Figure 4.2 represent what we should expected. On the left, reducing the base size the result converges to the Richardson Extrapolation value. On the right, there is the decreasing relative error with respect to the extrapolated value.

- **Number of prism layers:** [5, 7, 10, 15]

The procedure we follow to study the effect of the number of prism layer on the result is almost the same. For this study we choose a different grid refinement ratio $r = 1.5$ and proceed to compute the higher order term with the Richardson Extrapolation. Also for this case the result meet the expectations, and is clearly noticeable the
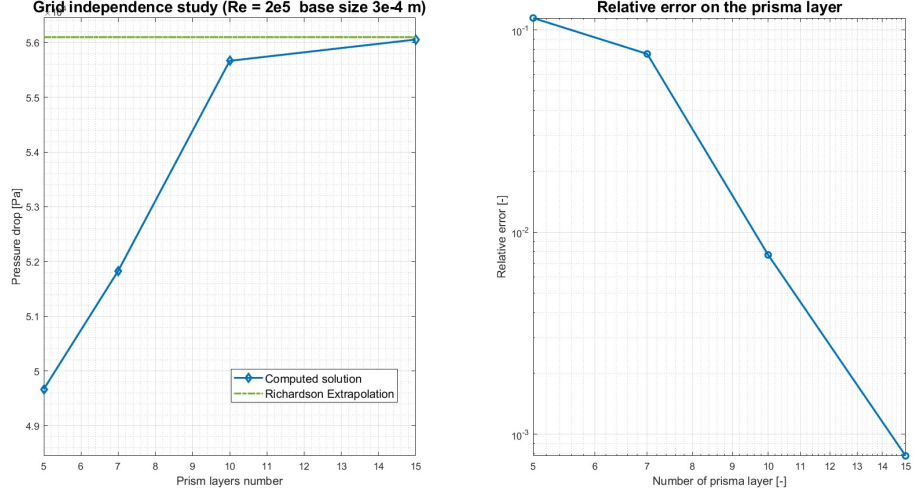

Figure 4.3: (a) Grid independence on the number of prism layers; (b) Relative error

convergence of our value.

For wall treatment, it was determined that a number of prism layers, set at 10, was enough for a good accuracy. Our model does not have a low Y+ imprint, but, as said before it is very important to ensure that Y+ does not overcome 5. In order to ensure this condition we changed the parameter "Near wall thickness" throughout all simulations. To concluded a consistent set of main parameters was employed:

- 1) Base size: 0.3 mm

- 2) Number of Prism Layers: 10

- 3) Surface Growth Rate: 1.15

These standardized parameters served as the foundation for ensuring uniformity and reliability across the study.
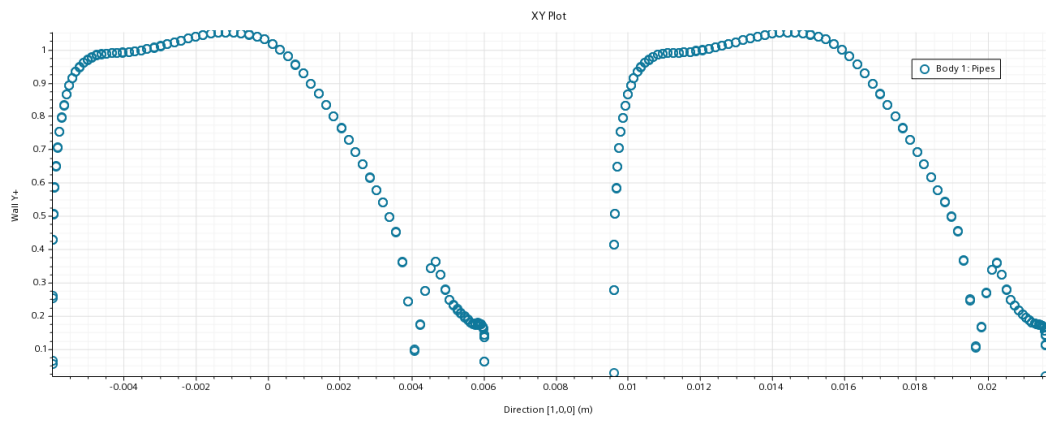
Figure 4.4: Plot Y+

Chapter 5

Results

Following the preliminary sections essential for accurate computations, this segment presents velocity and pressure profiles. Subsequently, it delves into the analysis of how the Friction Factor behaves in relation to Reynolds numbers.

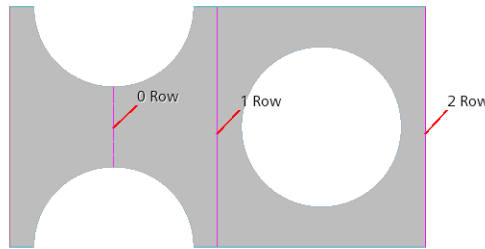## 5.1 Velocity and Pressure Drop

Figure 5.1: Section for plot

Assuming the no-slip condition hypothesis, at the points where the fluid comes into contact with the pipes, the flow velocity drops to zero, creating the characteristic curves illustrated in the Figure 5.3.

As expected the maximum velocity is obtained along the space between two pipes of the same column. In Figure 5.3 this is represented by the '0 Row' curve, which, as previously explained, corresponds to a plane situated between the first two pipes. Then, as the flow encounter the staggered pipe, due to the no-slip condition, there is a minimum of the velocity.

In the context of pressure, the maximum of the latter is present in the first point encountered horizontally by the flow with the pipe (stagnation point, where total condition are considered), another pick is between the first two pipes, after the staggered configuration there is a decreasing of the pressure.
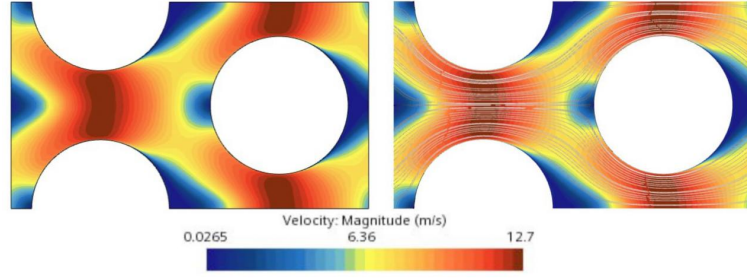
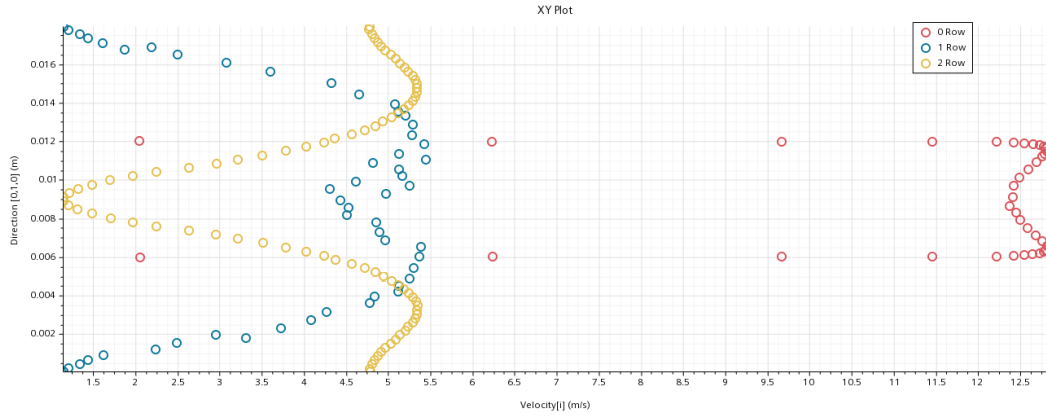**Figure 5.2:** Plot of velocity and streamlines

Figure 5.3: Plot of velocity along three different section: between two pipes, after two pipes and after the staggered configuration. Re=2E05

From Fig.5.4, it is possible to note that, as discussed before, globally, pressure undergoes a local rise in '0 Row' section and then increases after a compression in divergent duct, finally, downstream the last pipe in the elementary cell we can see a global decrease. In particular, as concerned the '0 Row' section note that the maximum of the pressure is located in the axis of the duct; similarly, in '1 Row section' the maximum of the pressure is always along the same axis of the '0 Row' section, but we can note a decrease of the pressure along the section were the wave (of initial pipes) is located. In turn the trend of the pressure in '2 Row' section informs us about a minimum of the pressure where the wave is located.
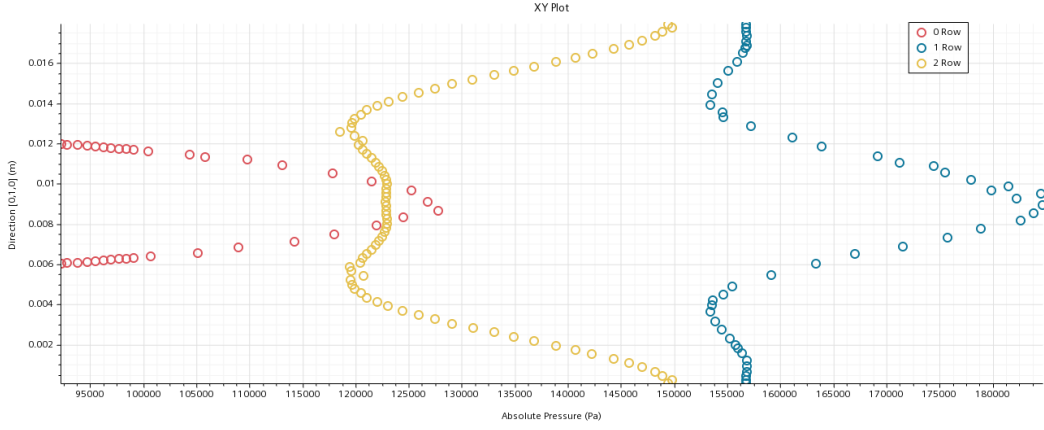
Figure 5.4: Plot of pressure along three different section: between two pipes, after two pipes and after the staggered configuration. Re=2E05
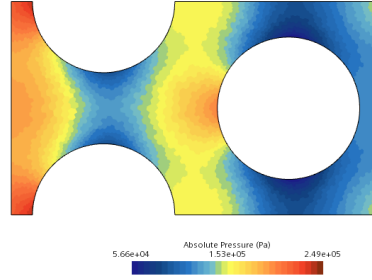

Figure 5.5: Scalar scene of absolute Pressure

5.2   Validation of Friction Factor

How said before, our main reference is the experimental work of Zukauskas [4] that provided experimental curves for our geometry. The equations by Incropera book permit us to calculate the friction factor starting from pressure drop and maximum velocity to compare with Zukauskas values:

$$f = \frac{\Delta P}{\frac{1}{2}\rho V_{max}^2 N \chi}$$

with:

- N = 2 (Number of rows);

- $\chi = 1.1$ from Re=1E05;

To remain as coherent as possible with the Incropera book, we use the same geometric correlation for the maximum velocity computed as follow $V_{max} = V_\infty \frac{S_T}{S_T - D}$

The amplitude of the error bar for Zukauskas correlation is of $\pm$ 10%. Instead, in order to make our error bar, we have calculated the GCI (Grid Convergence Index) for every Reynolds number, so, to do this, for every Reynolds number we have simulated three different situation changing with the base size
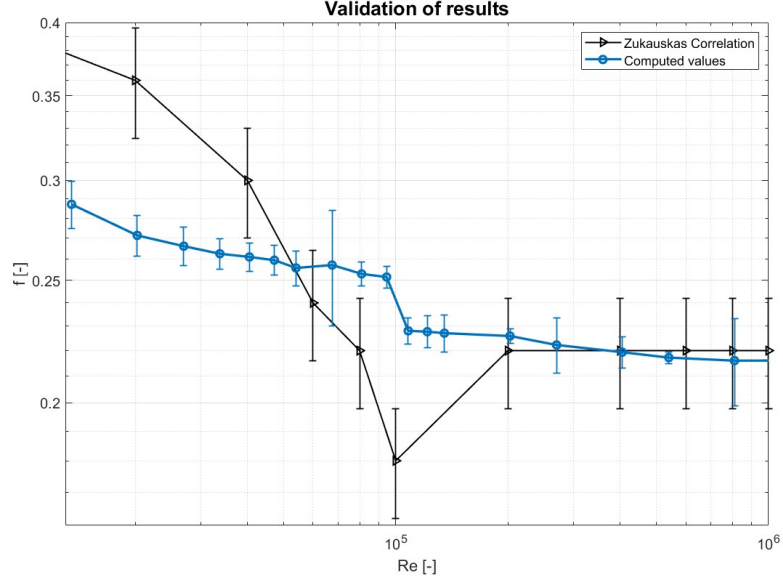

Figure 5.6: Computed friction factor values compared to Zukauskas values

It is possible to note that our trend do not intersect the error bar for small Reynolds number , but for high Reynolds number our model intersect very well the experimental values. It is possible to explain this behaviour remembering that our turbulent model is an 'higher Reynolds model', so became very precise with higher Reynolds number.

15

Chapter 6

Conclusion

In this report, we analyzed how the friction factor varies with changes in the Reynolds number within a staggered tube bank. Water was selected as the fluid for simulations, with its properties assumed to remain constant throughout. Our STAR-CCM+ setup involved defining a geometry that leveraged the symmetric characteristics of the tube bank while ensuring a fully developed state to account for the periodic nature of our case. We opted for the realizable two layer k-ϵ model to address turbulence issues near curved walls and adverse pressure gradient. Regarding mesh setup, once the model was chosen, we conducted a grid independence study on base size and prism layers to determine optimal values. As expected the simulations revealed notable findings, including stagnation zones associated with velocity and pressure changes in the approaching areas of the main stream encountering the pipes. Our analysis indicated that the calculated friction factor closely matches the theoretical predictions derived from Zukauska's experiments above all for high number of Reynolds.

Bibliography

[1]   ANSYS. *4.4.3 Realizable k- ε Model*. `https : / / www . afs . enea . it / project / neptunius/docs/fluent/html/th/node60.htm`. [Accessed 17-02-2024].

[2]   Frank P Incropera, David P DeWitt, and D P Dewitt. *Fundamentals of heat and mass transfer*. 3rd ed. John Wiley and Sons (WIE), July 1990, p. 437.

[3]   Tsan-Hsing Shih, Jiang Zhu, and John L. Lumley. «A new Reynolds stress algebraic equation model». In: *Computer Methods in Applied Mechanics and Engineering* 125.1–4 (Sept. 1995), pp. 287–302. ISSN: 0045-7825. DOI: `10 . 1016 / 0045 - 7825(95) 00796-4`. URL: `http://dx.doi.org/10.1016/0045-7825(95)00796-4`.

[4]   A. Zukauskas. *Heat Transfer from Tubes in Crossflow*. 1998.